

# LLM-Assisted Multi-Teacher Continual Learning for Surgical Visual Question Answering

Yuyang Du<sup>†</sup>, Kexin Chen<sup>†</sup>, Yue Zhan, Chang Han Low, Tao You, Mobarakol Islam, Ziyu Guo, Yueming Jin\*, Guangyong Chen, Pheng Ann Heng

**Abstract**—Visual question answering (VQA) is crucial for promoting surgical education. In practice, the needs of trainees are constantly evolving, such as learning more surgical types, adapting to different robots, and learning new surgical instruments and techniques for various surgeries. However, patient data privacy often restricts the availability of old data when updating the model, necessitating an exemplar-free continual learning (CL) setup. Prior CL studies overlooked two vital problems in the surgical domain: i) large domain shifts from diverse surgical operations collected from multiple sources, and ii) severe data imbalance arising from the uneven presence of surgical instruments or activities. This paper proposes addressing these problems with a multimodal large language model (LLM) and an adaptive weight assignment methodology. We first develop a new multi-teacher CL framework that leverages a multimodal LLM as the additional teacher. The strong generalization ability of the LLM can bridge the knowledge gap when domain shifts and data imbalances occur. We then put forth a novel data processing method that transforms complex LLM embeddings into logits compatible with our CL framework. We further design an adaptive weight assignment approach that balances the generalization ability of the LLM and the domain expertise of the old CL model. Finally, to comprehensively test the effectiveness of our proposed method, we have also constructed two new surgical VQA datasets that are largely different from existing ones and could be valuable resources for future research. Extensive experimental results on the tested datasets demonstrate the superiority of our method to other advanced CL schemes.

**Index Terms**—Surgical education, visual question answering, continual learning, multi-modal large language model

## I. INTRODUCTION

High-quality surgical education plays a pivotal role in the professional development of clinical students, as it equips them with the necessary knowledge and skills to perform complex procedures and deliver high-quality patient care. However, traditional teaching methods, such as lectures and textbooks, may not always sufficiently address the diverse questions and

concerns that students encounter during their learning process. Furthermore, expert surgeons, who serve as the primary source of surgical knowledge, may not always be available to provide immediate feedback due to their demanding clinical and academic responsibilities [1]–[3]. In recent years, surgical visual question answering (VQA) models have garnered significant research interest [4]–[6]. These models are typically trained using expert demonstration videos or related images, and they can provide students with instant access to expert knowledge, enabling them to clarify their doubts and deepen their understanding of surgical procedures. Moreover, the integration of VQA models into intelligent systems enhances their ability to comprehend and interpret surgical scenes, thus laying the foundation for the future development of clinical assistance technologies like advanced surgical robots [7]–[10].

In surgical VQA, the needs of trainees are constantly evolving, such as learning more surgical types and adapting to different clinical systems. Meanwhile, new techniques and instruments are consistently introduced to enhance patient care. These introduce new environments (i.e., new surgical scenes) and new question-and-answer sets, leading to various new VQA tasks. Continual Learning (CL) ability on new tasks is highly crucial in developing advanced VQA systems. Conventional machine learning methods are likely to suffer from significant performance degradation on prior tasks when acquiring new knowledge, also known as catastrophic forgetting [11]. Pioneering works in the medical domain addressed this problem by adapting CL algorithms of general domain [12], [13]. For example, [12] developed a replay-oriented CL algorithm for medical image analysis. These studies are exemplar-based, where old patient data is accessible when updating the model. However, in realistic surgical VQA, it is preferable to incorporate new knowledge from multiple sources with more data, such as multiple clinical centers; due to high storage costs, data privacy restrictions, and licensing issues across different centers, exemplar-based methods are not practical.

Some recent works also focus on CL studies under the data privacy restriction. [14] adapted non-exemplar-based CL algorithms like Learning without Forgetting (LwF) [15] and Elastic Weight Consolidation (EWC) [16] in medical tasks. [17] introduced CL algorithms in instrument and tissue localization tasks alongside VQA, with a special focus on overlapping classes that appear in both the new dataset and the old one. However, we identified two main properties in the surgery domain that have been largely overlooked in the existing literature, leading to their unreliable performance when tackling complex surgical VQA tasks. The two properties include *large domain shift* and *severe data imbalance*.

Y. Du is with the Department of Information Engineering, the Chinese University of Hong Kong (CUHK), Hong Kong SAR, China

K. Chen, Z. Guo, and P. A. Heng are with the Department of Computer Science Engineering, CUHK, Hong Kong SAR, China. P. A. Heng is also with the Institute of Medical Intelligence and Extended Reality, CUHK, Hong Kong SAR, China

Y. Zhan is with the Department of Electrical and Electronic Engineering, the University of Hong Kong (HKU), Hong Kong SAR, China

C. Low is with the Department of Biomedical Engineering, National University of Singapore (NUS), Singapore

T. You is with the Department of Mathematics, NUS, Singapore

M. Islam is with the Department of Medical Physics and Biomedical Engineering, University College London (UCL), London, UK

Y. Jin is with the Department of Electrical and Computer Engineering, NUS, Singapore

G. Chen is with Zhejiang Lab, Zhejiang, China

\*Yueming Jin (ymjin@nus.edu.sg) is the corresponding author.

<sup>†</sup>Yuyang Du and Kexin Chen are equal contributors.

**Domain Shift:** When updating a CL model under the classic teacher-student framework, the model trained on old data (teacher) serves as an important reference for the new model. The new model (student) utilizes the logits of the old model during training, allowing the retention of the former’s knowledge without revisiting any old data [18]. If a teacher encounters an entirely unfamiliar task in the new training data, it just provides random guesses for the student’s reference [19], [20], referred to as the domain shift. In surgical applications, such domain shift is notably prevalent: surgical scenes from different types of surgeries show a large variety of appearances, even within specific categories like abdominal surgery, due to differences in instruments and surgical actions. For example, data for the surgery performed on a liver largely diverges from that on a kidney. The data collected from multiple sources may further increase this problem, given variations in operation protocols and clinical systems. This severe domain shift commonly exists in surgical datasets and significantly reduces the performance of the CL model, as the student learns nothing but the teacher’s random guesses.

**Data Imbalance:** In practical surgeries, some actions or instruments are less frequently presented. For example, the action of tissue manipulation frequently appears in many surgical datasets, given that most operations involve tissue interaction. Cutting action is also widely mentioned, especially in the dataset focusing on nephrectomy, while stapling is rarely mentioned in the same dataset because stapling is generally performed only after vessel cutting, a niche operation inside the whole nephrectomy. In training data, if some classes have significantly fewer examples than others, we identify this as data imbalance [21], [22]. Prior CL algorithms [12]–[17] did not particularly address imbalanced data, making the model inadequately trained for minor classes.

This paper leverages the strong generalization ability of multimodal large language models (LLMs) to overcome the knowledge limitations imposed by the two problems. Multimodal LLMs are generative AI models trained on vast amounts of image and text data collected across various domains [23]–[26]. Recently, they have received increasing interest in various research fields due to their ability to answer questions across diverse domains. Importantly, state-of-the-art LLMs have demonstrated promising competency in answering questions for the medical domain [27], [28]. This motivates us to utilize LLM-generated answers to fill the knowledge gap when training data exhibits new knowledge unfamiliar to the teacher model or is extremely imbalanced. An intuitive explanation is that, when faced with knowledge outside the teacher’s expertise, leveraging the robust medical understanding of an LLM is far superior to relying on the teacher model’s poorly trained knowledge (for imbalanced data) or even random guesses (for domain shifts).

Apart from the LLM-aided multi-teacher CL framework, this paper also devises an adaptive weight assignment approach to balance insights from the LLM’s general knowledge and the conventional teacher’s domain-specific expertise. With adaptive weights, the student training process reaches an ideal state: it takes more insights from the conventional teacher when the knowledge belongs to a familiar domain and is well-

trained with rich data; otherwise, it relies more on the LLM.

Furthermore, we construct two new surgical VQA datasets to validate our innovations in real-world surgical settings. We developed a novel GPT-based QA pair generation method when building the new VQA dataset. We apply in-context learning (ICL) [29]–[33], an advanced few-shot learning method, for better analysis of text descriptions for a clinical image.

We summarize the contributions of this paper as follows:

- 1) We put forth an LLM-assisted multi-teacher CL framework and developed a novel processing scheme to extract logits from an LLM, providing a valuable reference for future efforts to leverage LLMs in CL studies.
- 2) We developed an adaptive weighting scheme that balances insights from the LLM’s generalization ability and the teacher’s domain expertise to improve the student training process. The scheme demonstrated a compelling performance under the proposed framework.
- 3) The two new surgical VQA datasets has been open-sourced, which provides a valuable data resource for future research. Furthermore, the building of the two VQA datasets also point out a novel way to generate QA pairs with ICL. Experiments across four datasets show the effectiveness of our method.

## II. PROPOSED METHOD

### A. Preliminaries

**Problem Formulation and Notations:** Let us assume a CL process with  $\tau$  time periods, in which  $t \in \{1, \dots, \tau\}$  denotes a time period of the process. We denote the training dataset in time  $t$  by  $D_t$ , wherein element  $d_{t,i} \in D_t$  represents the  $i^{\text{th}}$  training sample for time  $t$ . Each training sample  $d_{t,i}$  contains a surgical frame and several closely associated clinical questions. We denote the classes appearing in  $D_t$  by  $C_t$ , wherein element  $c_{t,j}$  represent the  $j^{\text{th}}$  class appearing in  $D_t$ . If class  $c_{t,j}$  frequently appears in  $D_t$  but never appears in previous training datasets (i.e.,  $D_{t-1}, D_{t-2}, \dots, D_1$ ), we say a domain shift happens at class  $c_{t,j}$ . Further, if the appearing frequency of class  $c_{t,j}$  is significantly smaller than other classes in  $D_t$ , then data imbalance happens at class  $c_{t,j}$ .

**Distillation Loss in Continual Learning:** In CL, knowledge is obtained from an infinite stream of data, with the goal of gradually updating the model with new data and avoiding forgetting the knowledge learned in old data. Knowledge distillation (KD) is an efficient approach for retaining the knowledge of the old model and addressing the catastrophic forgetting problem without revisiting the previous training data [34]. There are three categories of KD: response-based KD, feature-based KD, and relation-based KD. In this paper, we focus on response-based KD because it is flexible and allows student and teacher models of different network types [35].

The distillation loss of the KD process is formulated as

$$L_{KD} = L_{CE} \langle \sigma(z^T/\delta), \sigma(z^S/\delta) \rangle \quad (1)$$

where  $L_{CE} \langle \cdot, \cdot \rangle$  denotes the cross-entropy loss;  $\sigma(\cdot)$  denotes the softmax function;  $z^T$  and  $z^S$  denote the output logits of the teacher and the student model, respectively;  $\delta$  is a

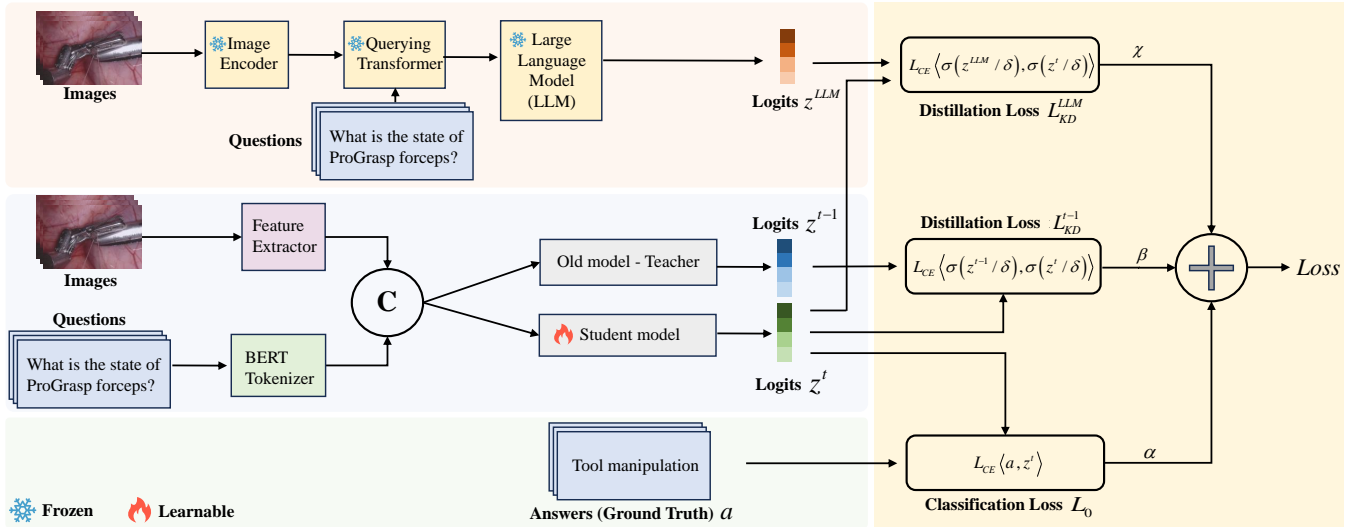


Figure 1: The proposed LLM-assisted multi-teacher CL framework. The model is used to process bimodal input (text and image) and provide predictions for the VQA task. The proposed weight adaption scheme (highlighted in the light orange zone) is designed to trade off the general knowledge of the LLM and the medical expertise of the previous CL model. The frozen LLM is highlighted in light red, while the conventional teacher and student models are highlighted in light blue. Ground truth lies in the light green zone.

temperature hyperparameter that controls the softness of the probability distributions. With  $\delta = 1$ , we get the standard softmax function, and as  $\delta$  increases, the produced probability distribution becomes softer, providing more information such as which class is more similar to the predicted class.

### B. Multi-teacher CL Framework with LLM

To overcome domain shifts and data imbalances, we introduce an additional multimodal LLM teacher with a strong generalization ability for better knowledge transfer. When the model in time  $t$  is unfamiliar with the knowledge in time  $t+1$ , the LLM teacher will guide the student to learn from a more reasonable knowledge source.

Our multi-teacher CL framework is presented in Fig. 1. As the figure shows, the general loss function  $L$  is written as

$$L = \alpha L_0 + \beta L_{KD}^{t-1} + \chi L_{KD}^{LLM} \quad (2)$$

where  $\alpha$ ,  $\beta$ , and  $\chi$  are normalized adaptive weights with a sum of one (see Section II-C for the weight assignment scheme);  $L_0$  is the cross-entropy loss supervised by the hard labels;  $L_{KD}^{t-1}$  is the KD loss between the new CL model trained in time  $t$  (i.e., the student model) and the old CL model trained in time  $t-1$  (i.e., the conventional teacher model);  $L_{KD}^{LLM}$  is the KD loss between the student model and the LLM teacher. In this paper, we denote the logits of the student model, the old teacher model, and the LLM teacher mode by  $z^t$ ,  $z^{t-1}$ , and  $z^{LLM}$ , respectively. And we write  $L_{KD}^{t-1}$  and  $L_{KD}^{LLM}$  as

$$L_{KD}^{t-1} = L_{CE} \langle \sigma(z^{t-1}/\delta), \sigma(z^t/\delta) \rangle \quad (3)$$

$$L_{KD}^{LLM} = L_{CE} \langle \sigma(z^{LLM}/\delta), \sigma(z^t/\delta) \rangle \quad (4)$$

Since the LLM teacher is implemented in a complex transformer network that is significantly different from the conventional teacher model and the student model, some

transformation works are needed to obtain the logits from the embeddings. We next give details about the selected LLM and the embedding-logit transformation as follows.

We select InstructBLIP [36], an open-source multimodal LLM with vision and language ability, as the LLM teacher. There are three components in InstructBLIP: one image encoder that deals with the image input, one text-in-text-out LLM to manage the output, and an image-text transformer to bridge the two modules. Thanks to the modular architectural design, InstructBLIP is highly flexible, and we can quickly adapt a wide range of text-to-text LLMs for implementation. Without loss of generality, we utilize FlanT5 [37], an instruction-tuned model based on Transformer T5, as the text-in-text-out LLM.

The embeddings we obtained from the last fully connected layer of FlanT5 is a self-attention matrix denoted by  $e_{LLM}$ . The size of  $e_{LLM}$  is  $N \times (M+1) \times P$ , where  $N$  is the number of classes in time  $t$ , i.e., the cardinality of  $C_t$ ;  $P$  is the LLM's vocabulary; and  $M$  is the number of tokens we used to represent each class label.<sup>1</sup> As presented in Eq. (4), the desired logits  $z^{LLM}$  should have a size of  $N \times 1$ . We now illustrate how we transform the  $N \times (M+1) \times P$  embeddings into the  $N \times 1$  logits.

As in Fig. 2, we first reshape the extracted embeddings and obtain a new matrix  $e_{LLM}^R$ . We conduct one-hot encoding and tokenization on the classification label set  $C^t$ . Note that  $e_{LLM}^R$  and  $C^T$  have the size of  $N(M+1) \times P$ . We then calculate the cross-entropy loss between  $e_{LLM}^R$  and  $C^T$  by

$$L_{CE}^I(i) = L_{CE} \langle e_{LLM}^R(i), C^T(i) \rangle \quad (5)$$

The resulting vector  $L_{CE}^I$  has a size of  $N(M+1) \times 1$ . We next reshape the vector to a  $N \times (M+1)$  matrix and conduct

<sup>1</sup>The second dimension of the matrix is  $M+1$  rather than  $M$  because we add one additional pause token for each word to indicate the end of a word.

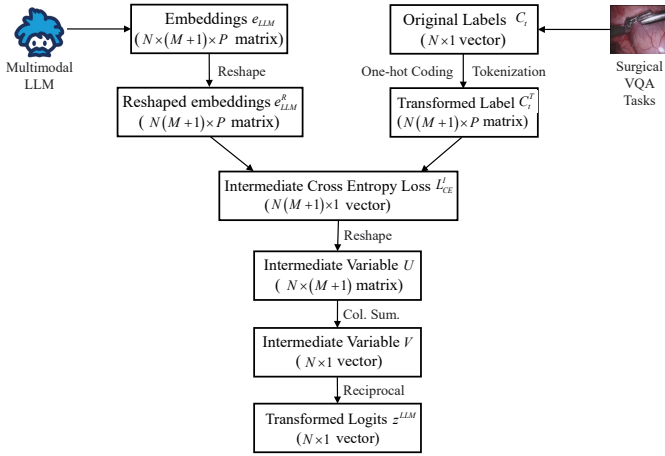


Figure 2: The workflow logits transformation after extracting the embeddings.

column summation to obtain the cross entropy corresponding to each label. In the resulting  $N \times 1$  vector  $V$ , element  $V(j)$  represents the expected loss of label  $c_{t,j}$ , which is negatively related to the probability of label  $c_{t,j}$  being selected as the final classification result. While in the desired logits vector  $z^{LLM}$ , element  $z^{LLM}(j)$  should be positively related to the classification probability of  $c_{t,j}$  so that  $\sigma(z^{LLM}/\delta)$ , the output of the softmax layer, can be a probability vector. Therefore, we need to further transform vector  $V$  to make its elements positively related to the classification probability. One possible way is to inverse the elements in  $V$ , i.e.,  $z^{LLM}(j) = 1/V(j)$ .

### C. Adaptive Weight Assignment

In Eq. (2),  $\alpha$ ,  $\beta$ , and  $\chi$  denote the weights of  $L_0$ ,  $L_{KD}^{t-1}$ , and  $L_{KD}^{LLM}$ , respectively. This paper adaptively adjusts  $\beta$  and  $\chi$  during the training process with the weight assignment approach described below and sets  $\alpha$  as a hyperparameter. Together the three items will jointly control the model optimization.

During the model training at time  $t$ , the severity of the domain shift of a medical dataset can be assessed by the old model’s classification accuracy on the training dataset  $D_t$ . If the old CL model achieves high accuracy on  $D_t$ , we infer it possesses familiarity with the knowledge in  $D_t$ . In contrast, if it has poor accuracy on  $D_t$ , say worse than the LLM teacher’s accuracy, we conclude the old CL model lacks reliable expertise for this training iteration. Given this rationale, we adjust  $\beta$  and  $\chi$  based on the relative accuracies of the CL teacher and LLM teacher on  $D_t$ . A greater accuracy differential indicates a more severe domain shift, so more weight should be assigned to the LLM to leverage its generalization ability and general knowledge in the medical domain.

In addition to mitigating domain shift, we aim to address the data imbalance present in the surgical-related dataset via adaptive weight. We observed a unique imbalance in the label distribution of the tested dataset, where some surgical operations and instruments were queried very frequently, while others were rarely mentioned. For instance, in a surgical dataset pertaining to nephrectomies, the action of cutting is frequently referenced, while mentions of stapling are relatively

rare because stapling is a specialized procedure performed only after vessel cutting, a niche operation within the broader context of nephrectomy. Although the old CL model may have some knowledge in these seldomly mentioned domains, its knowledge grasp is far from expert due to the scarcity of training data. In such cases, we give the LLM teacher a higher weight to help the training process use its general medical insights to fill in the knowledge gap.

With the above discussion, we see that the assignments of  $\beta$  and  $\chi$  are jointly decided by domain shifts and data imbalances. Therefore, we express  $\beta$  and  $\chi$  as

$$\beta = \theta_{DS}\beta_{DS} + \theta_{DI}\beta_{DI} \quad (6)$$

and

$$\chi = \theta_{DS}\chi_{DS} + \theta_{DI}\chi_{DI} \quad (7)$$

where we assume that hyperparameters  $\theta_{DS}$  and  $\theta_{DI}$  satisfy  $\theta_{DS} + \theta_{DI} = 1 - \alpha$ , reflecting the importance of domain shift (DS) and data imbalance (DI) in our model training, respectively. If we want the model training process focus more on domain shift, we increase  $\theta_{DS}$  and decrease  $\theta_{DI}$ ; on the other hand, if we want the training process focuses more on data imbalance, we operate conversely. Further,  $\beta_{DS}$  and  $\chi_{DS}$  in Eq. (6) and Eq. (7) denote the weight share of the old CL teacher and the LLM teacher in terms of domain shifts, respectively;  $\beta_{DI}$  and  $\chi_{DI}$  denote the weight share of the two teachers in terms of data imbalance. To have  $\beta + \chi = 1 - \alpha$ , we need to make sure

$$\beta_{DS} + \chi_{DS} = 1 \quad (8)$$

and

$$\beta_{DI} + \chi_{DI} = 1 \quad (9)$$

We now detail how we assign  $\beta_{DS}$  and  $\chi_{DS}$ . We know that  $\beta_{DS}$  and  $\chi_{DS}$  are assigned according to the accuracies of the old CL teacher and the LLM teacher on  $D_t$ . Given  $D_t$ , let us denote the classification accuracy of the CL model in time  $t-1$  and that of the LLM by  $acc_{t-1}$  and  $acc_{LLM}$ , respectively. To fulfill the constraint in Eq. (8) and Eq. (9), we let  $\beta_{DS}$  and  $\chi_{DS}$  be

$$\beta_{DS} = \frac{acc_{t-1}}{acc_{t-1} + acc_{LLM}} \quad (10)$$

and

$$\chi_{DS} = \frac{acc_{LLM}}{acc_{t-1} + acc_{LLM}} \quad (11)$$

The domain shift problem can be well addressed with the assignment scheme in Eq. (10) and Eq. (11), as the LLM will be given a higher weight when the old CL model is random guessing.

We next introduce how  $\beta_{DI}$  and  $\chi_{DI}$  are decided. In time  $t$ , we denote the set of previously appeared data by  $D_{t,\dots,1}$  (i.e.,  $D_{t,\dots,1} = D_t \cup D_{t-1} \dots \cup D_1$ ). The  $k^{th}$  class labels in  $D_{t,\dots,1}$  are denoted by  $c_k$ , and the appearance time of  $c_k$  is denoted by  $d_k$ . To evaluate the data imbalance in  $D_{t,\dots,1}$ , we introduce the concept of imbalance ratio as in [38], which is

$$IR = \max(d_k)/\min(d_k) \quad (12)$$

It is important to note that  $d_k$  in Eq. (12) cannot be zero given its definition described above.

Under the constraint in Eq. (8) and Eq. (9), we design  $\beta_{DI}$  and  $\chi_{DI}$  as

$$\beta_{DI} = \frac{1}{1 + \log_N IR} \quad (13)$$

and

$$\chi_{DI} = \frac{\log_N IR}{1 + \log_N IR} \quad (14)$$

where  $N$  is a hyperparameter.

From Eq. (13) and Eq. (14), we can see that when the data is severely imbalanced, we have a large  $\chi_{DI}$  so that the LLM's general domain knowledge can be well utilized to fill the knowledge gap. The data imbalance problem can be well alleviated.

Finally, we give the expression of  $\beta$  and  $\chi$  as follows:

$$\beta = \theta_{DS} \frac{acc_{t-1}}{acc_{t-1} + acc_{LLM}} + \theta_{DI} \frac{1}{1 + \log_N IR} \quad (15)$$

and

$$\chi = \theta_{DS} \frac{acc_{LLM}}{acc_{t-1} + acc_{LLM}} + \theta_{DI} \frac{\log_N IR}{1 + \log_N IR} \quad (16)$$

### III. EXPERIMENTS AND ANALYSIS

#### A. Dataset

We design our continual procedure using four datasets to simulate a realistic VQA CL scenario, including function-incremental learning with a broader range of questions and answers, and scene-incremental learning with a greater variety of surgical types: we train our CL model with EndoVis17 at  $t = 1$ , with EndoVis18 at  $t = 2$ , and then with DAISI-VQA at  $t = 3$ , and finally with LRSP-VQA at  $t = 4$ . The first two datasets are well-known open-source datasets used in previous papers [39]–[41], while the last two datasets are the new ones we developed with the assistance of GPT-3.5. We first give an overview of the four datasets, and then elaborate on the generation method for DAISI-VQA and LRSP-VQA.

**EndoVis17** is derived from a public challenge dataset on robotic abdominal surgery [42]. The QA pairs in this dataset have single-word answers categorized as either surgical actions or instrument locations. In our experiments, 5 videos are used, obtaining 73 frames with 376 QA pairs in the training set, and 24 frames with 96 QA pairs in the testing set.

**EndoVis18** is also derived from a public challenge dataset on robotic abdominal surgery [1]. Apart from action-related and location-related questions asked in EndoVis17, this dataset also includes questions related to organs, introducing domain shift at  $t = 2$ . Further, EndoVis18 considers additional 5 types of actions (i.e., looping, suction, clipping, staple, and suturing), significantly adding to the data imbalance. 14 videos are used where the training set contains 1560 frames with 9014 QA pairs. The test set has 447 frames with 2769 QA pairs.

**DAISI-VQA** is a new VQA dataset built upon the DAISI dataset reported in [43]. The original DAISI dataset contains images and instructional texts of various surgical procedures on different organs, with each procedure illustrated by multiple images and corresponding instructional texts.

For the QA pair generation, we first cleaned the original DAISI dataset by removing irrelevant images (such as frames

not containing any surgical content) and unimportant descriptions (such as those describing the hospital or the surgeon). We then generated QA pairs according to the text description for each image. To generate reasonable question(s) and reliable answer(s) for each image, we processed the text description of each image with GPT-3.5 and applied in-context learning (ICL), an advanced few-shot learning method tailored to LLMs [29]. Specifically, we provided GPT-3.5 with a prompt containing several example QA pairs to demonstrate how surgical questions should be asked and how answers can be inferred from the related text descriptions. Following these example QA pairs, the detailed description of a new, unaddressed DAISI image was appended to the prompt, and we then asked GPT-3.5 to generate QA pairs according to the textual description we provided. With strong reasoning and imitation abilities, GPT-3.5 analyzed the previously given examples, extrapolated the underlying task, and provided reasonable QA pairs for the given description.

In our DAISI-VQA dataset, there are 353 surgical images and 545 QA pairs. We assigned approximately 80% of the data for training and used the remaining data for testing.

**LRSP-VQA** refers to the Live Recorded Surgical Procedures VQA dataset we built with 36 video demonstrations about robotic-assisted surgical operations. These videos were collected from YouTube and WebSurg and were selected based on their in-video narration of the surgical procedures and the quality of the recording. We segmented the selected videos into 150 shorter parts, with each video snippet corresponding to one surgical phase within the whole procedure. The main purpose of this operation was to ensure that each segment contained the same set of surgical instruments throughout. Subsequently, we extracted frames from each video segment and obtained a total of 10,438 images from the 150 video segments. In the third step, we filtered out relevant portions of the video transcriptions corresponding to each specific video segment. These textual transcriptions contained the surgical instructions and explanations that were provided audibly in the video and could therefore serve as valuable descriptions for these selected surgical videos. With all images and textual descriptions obtained above, we leveraged GPT-3.5 for QA pair generation in a way similar to the QA pair generation in DAISI-VQA.

In LRSP-VQA, there are 1,136 QA pairs, and each QA pair has an associated surgical image. We assigned approximately 80% of the data for training and used the remaining data for testing.

After a brief introduction to each individual dataset, we now present Table I, which provides a detailed comparison of the four datasets in terms of the organ(s) and procedure(s) involved, surgical assisting system(s) applied, and surgical instruments used. This comparison can help readers better understand the significant data diversity we introduced in the two new datasets, which plays a vital role in validating our model's performance under severe domain shift and data imbalance. The comparison results are as follows:

- 1) **Organ**: Our two new datasets show much higher diversity in terms of organs involved in surgical QA pairs: QA pairs in DAISI-VQA and LRSP-VQA discuss 25 and

Table I: Data diversity (EV17, EV18, D-V, L-V represent EndoVis17, EndoVis18, DAISI-VQA, LRSP-VQA, respectively).

	EV17	EV18	D-V	L-V
<b>Organ</b>	kidney	kidney	abdomen, arm, axilla, brain, eye, eye orbit, cranial cavity, female reproductive, gastrointestinal, gluteal region, hand, heart, inguinal region, jaw, kidney, lung, male reproductive, nasal cavity, neck, oral cavity, parotid gland, retropharyngeal space, pelvis, submandibular region, thigh	abdomen, colon, female reproductive, kidney, lung, prostate, stomach
<b>Procedure</b>	nephrectomy	nephrectomy	/	gastrectomy, hysterectomy, lobectomy, nephrectomy, nephroureterectomy, prostatectomy, resection, thrombectomy, total mesorectal excision
<b>Surgical Assisting System</b>	Da-Vinci XI	Da-Vinci X, Da-Vinci XI	No surgical assisting system involved, all operations are manually conducted	Da-Vinci X, Da-Vinci XI, Da-Vinci SI, Da-Vinci SP, Hugo RAS
<b>Instrument</b>	bipolar forceps, large needle driver, monopolar curved scissors, prograsp forceps, ultrasound probe	bipolar forceps, clip applier, large needle driver, monopolar curved scissors, prograsp forceps, stapler, suction, ultrasound probe	suture, suction, scissors, probe, needle, loop, driver, forceps, sutures, blade, ultrasound, tube, pusher, scalpel, stapler, passer, saw, clamps, wires, clamp, anesthetic, remover, advancement, forceps, bone-cutters, tourniquet, inserter, ureter, mallet, adhesive, strips, mesh	bovie cauter, cadier forceps, cold scissors, suction irrigator, monopolar curved scissors, curved bipolar dissector, endo grasp, endo shears, fenestrated bipolar forceps, long bipolar graspers, maryland bipolar forceps, needle driver, vessel sealer, permanent cautery hook, prograsp forceps, stapler, thoracoscopic rib cutter, tip up fenestrated graspers, permanent cautery spatula

7 different organs, respectively, while previous datasets (i.e., EndoVis17 and EndoVis18) focus on the kidney only.

- 2) **Surgical procedure:** EndoVis17 and EndoVis18 only consider nephrectomy, while our LRSP-VQA investigates eight additional clinical procedures apart from nephrectomy. For DAISI-VQA, although the detailed information about clinical procedures cannot be directly extracted from the original DAISI dataset, we note that the number of clinical procedures in DAISI-VQA obviously exceeds that of LRSP-VQA, given its large number of organs investigated.
- 3) **Surgical assisting system:** Many surgical VQA datasets are built with videos recorded by surgical robots. For example, the surgical operation in EndoVis17 is completed by the Da Vinci X robotic surgical system [44], while the later-released EndoVis18 applies a more advanced Da Vinci Xi platform [45] when building the dataset. For our datasets, LRSP-VQA introduces two of the latest robotic surgical systems in the Da Vinci series (i.e., Da Vinci Si [46] and Da Vinci SP [47]) and a robotic surgical system from a new series (the Hugo RAS platform [48]). For the DAISI-VQA dataset, all surgical operations are manually conducted, which also differs significantly from EndoVis17 and EndoVis18 developed in previous works.
- 4) **Instruments:** Our two new datasets show much higher diversity in terms of instruments involved in surgical QA

pairs: QA pairs in DAISI-VQA and LRSP-VQA use 31 and 19 different instruments, respectively, while previous datasets involve fewer instruments, with EndoVis17 and EndoVis18 discussing 5 and 8 surgical instruments, respectively.

From the above discussion, it is evident that our new datasets are significantly different from those developed previously, and an obvious domain shift can be introduced when these two datasets are applied at  $t = 3$  and  $t = 4$ . The two datasets developed in this paper also contribute to the diversity of the data sources in surgical VQA research.

### B. Baselines and Implementation Details

We evaluate our approach in comparison to the following algorithms under a CL setting:

- 1) **Fine Tune (FT):** FT is a straightforward adaptation strategy in CL. In FT, a model trained on previous tasks is updated with new data. Although FT can quickly adapt to new tasks, it often suffers from catastrophic forgetting. Therefore, FT is always expected to have the worst average performance under a CL setting [49].
- 2) **Experience Replay (ER):** ER mitigates catastrophic forgetting by storing the original training data in a memory buffer. When the model is trained on new tasks, it revisits examples from this memory buffer, thus remembering the old tasks [50]. Although ER has an ideal performance

Table II: Benchmarking experiments - Accuracy.

	Accuracy ( $t = 1$ to $t = 2$ )			Accuracy ( $t = 2$ to $t = 3$ )				Accuracy ( $t = 3$ to $t = 4$ )				
	EV17	EV18	Avg.	EV17	EV18	D-V	Avg.	EV17	EV18	D-V	L-V	Avg.
FT	0.2917	0.5905	<u>0.4411</u>	0.0938	0.3286	0.7632	<u>0.3952</u>	0.1250	0.1123	0.4561	0.6953	<u>0.3472</u>
ER	0.5417	0.5782	<u>0.5599</u>	0.5313	0.6071	0.7544	<u>0.6309</u>	0.5313	0.5544	0.7018	0.6652	<u>0.6131</u>
LwF	0.4479	0.5309	<u>0.4894</u>	0.3229	0.4124	0.6930	<u>0.4761</u>	0.0938	0.1217	0.6842	0.5880	<u>0.3719</u>
Online-EWC	0.4167	0.5002	<u>0.4584</u>	0.0625	0.3611	0.7368	<u>0.3868</u>	0.1250	0.1116	0.7018	0.6910	<u>0.4073</u>
EWC++	0.4792	0.4680	<u>0.4736</u>	0.0938	0.3734	0.7105	<u>0.3926</u>	0.1250	0.1098	0.5877	0.6781	<u>0.3751</u>
<b>Our Method</b>	<b>0.5104</b>	<b>0.5619</b>	<b><u>0.5362</u></b>	<b>0.3229</b>	<b>0.4709</b>	<b>0.7368</b>	<b><u>0.5102</u></b>	<b>0.1146</b>	<b>0.3254</b>	<b>0.6140</b>	<b>0.6223</b>	<b><u>0.4191</u></b>

Table III: Benchmarking experiments - F-score.

	Accuracy ( $t = 1$ to $t = 2$ )			Accuracy ( $t = 2$ to $t = 3$ )				Accuracy ( $t = 3$ to $t = 4$ )				
	EV17	EV18	Avg.	EV17	EV18	D-V	Avg.	EV17	EV18	D-V	L-V	Avg.
FT	0.1843	0.3806	<u>0.2825</u>	0.0327	0.0982	0.8751	<u>0.3353</u>	0.0436	0.0425	0.2088	0.5153	<u>0.2026</u>
ER	0.3344	0.3681	<u>0.3512</u>	0.2784	0.3792	0.8721	<u>0.5099</u>	0.3048	0.2740	0.8440	0.4825	<u>0.4763</u>
LwF	0.3034	0.2966	<u>0.3000</u>	0.1682	0.1870	0.8419	<u>0.3990</u>	0.0580	0.0579	0.2807	0.4118	<u>0.2021</u>
Online-EWC	0.2276	0.2012	<u>0.2144</u>	0.0362	0.1316	0.8648	<u>0.3442</u>	0.0400	0.0427	0.2400	0.5229	<u>0.2114</u>
EWC++	0.2229	0.2624	<u>0.2427</u>	0.0532	0.1922	0.7293	<u>0.3249</u>	0.0400	0.0339	0.2059	0.4963	<u>0.1940</u>
<b>Our Method</b>	<b>0.3091</b>	<b>0.3185</b>	<b><u>0.3138</u></b>	<b>0.2106</b>	<b>0.2556</b>	<b>0.8576</b>	<b><u>0.4413</u></b>	<b>0.0483</b>	<b>0.1302</b>	<b>0.4189</b>	<b>0.4577</b>	<b><u>0.2638</u></b>

Table IV: Ablation study - Accuracy.

	Accuracy ( $t = 1$ to $t = 2$ )			Accuracy ( $t = 2$ to $t = 3$ )				Accuracy ( $t = 3$ to $t = 4$ )				
	EV17	EV18	Avg.	EV17	EV18	D-V	Avg.	EV17	EV18	D-V	L-V	Avg.
Scenario 1	0.4271	0.5677	<u>0.4974</u>	0.1042	0.3337	0.7456	<u>0.3945</u>	0.1250	0.1123	0.5877	0.6824	<u>0.3769</u>
Scenario 2	0.4063	0.5702	<u>0.4882</u>	0.0938	0.2376	0.7632	<u>0.3648</u>	0.0938	0.0841	0.4123	0.6352	<u>0.3063</u>
Scenario 3	0.4167	0.5670	<u>0.4918</u>	0.1042	0.3182	0.7807	<u>0.4010</u>	0.1042	0.1051	0.4211	0.6352	<u>0.3164</u>
Scenario 4	0.4479	0.5309	<u>0.4894</u>	0.3229	0.4124	0.6930	<u>0.4761</u>	0.0938	0.1217	0.6842	0.5880	<u>0.3719</u>
<b>Our Method</b>	<b>0.5104</b>	<b>0.5619</b>	<b><u>0.5362</u></b>	<b>0.3229</b>	<b>0.4709</b>	<b>0.7368</b>	<b><u>0.5102</u></b>	<b>0.1146</b>	<b>0.3254</b>	<b>0.6140</b>	<b>0.6223</b>	<b><u>0.4191</u></b>

Table V: Ablation study - F-score.

	Accuracy ( $t = 1$ to $t = 2$ )			Accuracy ( $t = 2$ to $t = 3$ )				Accuracy ( $t = 3$ to $t = 4$ )				
	EV17	EV18	Avg.	EV17	EV18	D-V	Avg.	EV17	EV18	D-V	L-V	Avg.
Scenario 1	0.2336	0.2365	<u>0.2351</u>	0.0319	0.0988	0.8673	<u>0.3327</u>	0.0400	0.0359	0.1651	0.5071	<u>0.1870</u>
Scenario 2	0.2595	0.3101	<u>0.2848</u>	0.0381	0.0825	0.8777	<u>0.3328</u>	0.0688	0.0383	0.1374	0.4126	<u>0.1643</u>
Scenario 3	0.2658	0.2883	<u>0.2770</u>	0.0313	0.0924	0.8871	<u>0.3369</u>	0.0362	0.0460	0.2478	0.424	<u>0.1887</u>
Scenario 4	0.3034	0.2966	<u>0.3000</u>	0.1682	0.1870	0.8419	<u>0.3990</u>	0.0580	0.0579	0.2807	0.4118	<u>0.2021</u>
<b>Our Method</b>	<b>0.3091</b>	<b>0.3185</b>	<b><u>0.3138</u></b>	<b>0.2106</b>	<b>0.2556</b>	<b>0.8576</b>	<b><u>0.4413</u></b>	<b>0.0483</b>	<b>0.1302</b>	<b>0.4189</b>	<b>0.4577</b>	<b><u>0.2638</u></b>

in a CL process, it may not always be possible in medical applications, given that storing previous patient data causes ethical problems. In this paper, we only use ER as a performance upper bound in the benchmarking.

- 3) **Learning without Forgetting (LwF)**: LwF is a famous CL algorithm that applies KD in the training process. By storing previous knowledge in a distilled model, the algorithm enables an efficient CL process that learns new knowledge without forgetting old ones [15].
- 4) **Elastic Weight Consolidation++ (EWC++)**: EWC++ is an enhanced version of the original EWC algorithm by automating the adjustment of weight importance and simplifying the calculation of the Fisher information matrix for better scalability and flexibility. [51]
- 5) **Online Elastic Weight Consolidation (Online-EWC)**: Online-EWC is also a much-improved variation of the

original EWC algorithm. It extends the original EWC algorithm by more efficiently updating the importance of model parameters to protect previously learned knowledge when new data arrives [52].

As for our method, its implementation details are as follows. At  $t = 1$ , we train the model on EndoVis17, using a learning rate of  $5 \times 10^{-6}$  and an epoch number of 60 (follow the settings in [42]). At  $t = 2$ , we train the model on EndoVis18, using a learning rate of  $5 \times 10^{-5}$  and an epoch number of 80 (follow the settings in [1]). At  $t = 3$ , we train the model on DAIS-VQA, using a learning rate of  $5 \times 10^{-6}$  and an epoch number of 80. Finally, at  $t = 4$ , we train the model on LRSP-VQA, using a learning rate of  $1 \times 10^{-5}$  and an epoch number of 80.

All the above algorithms are implemented using PyTorch and trained with an NVIDIA Tesla T4 GPU. Adam optimizer is used throughout the experiments.



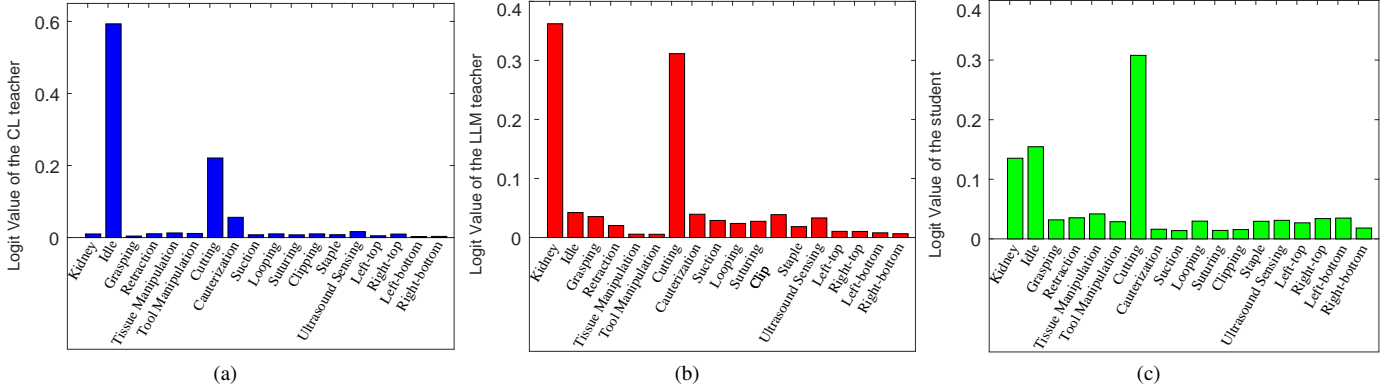


Figure 3: Logits of CL teacher, LLM teacher, and the student for the case in Fig. 4b.

### C. Experimental Results

Before a detailed analysis, it is important to clarify that our comparison focuses on a model’s *average* performance (specifically, accuracy and F-score) across all datasets tested at different times, rather than its performance on an individual dataset. This is because a bad CL model suffering from catastrophic forgetting might perform well on one dataset but falter on previously encountered ones. Conversely, a robust CL model maintains consistently high performance across all datasets. Although a good CL model may not outshine a bad one in a singular dataset, it demonstrates superior performance on average. In light of this, comparing average performance across all tested datasets is a tradition in CL studies [1], [12], [13], [42], and this paper follows the same setting.

We now take a look at the benchmarking results depicted in Table II and Table III. As expected, FT meets the severest catastrophic forgetting among all tested methods and gets the worst performance. Despite ER, the ideal upper bound, our technique consistently displays superior performance throughout the process. Compared with previous methods, our method improves the model accuracy of the second-best model by 9.56% at  $t = 2$ , 7.17% at  $t = 3$  and 2.90% at  $t = 4$ . We improve the F-score of the second-best model by 5.64%, 10.58% and 24.8% at  $t = 2$ ,  $t = 3$  and  $t = 4$ , respectively.

The above results prove our method’s remarkable ability in learning new knowledge without forgetting the old one. We attribute the good performance of the model to 1) the application of LLM in the training process for overcoming domain shift and data imbalance, and 2) the dynamic weight adjustment scheme that makes a good balance between the expert teacher model and the LLM. To demonstrate the efficacy of each component in the proposed method, we now carry out an ablation study. The following scenarios are considered within the ablation study:

- 1) In weight assignment, ignore data imbalance and consider domain shift only (i.e.,  $\theta_{DI} = 0$  and  $\theta_{DS} = 1$ ).
- 2) In weight assignment, ignore domain shift and consider data imbalance only (i.e.,  $\theta_{DI} = 1$  and  $\theta_{DS} = 0$ ).
- 3) Remove the entire adaptive weight assignment mechanism, opting instead for a fixed weight in the CL process.
- 4) Remove the LLM teacher and use the old CL model as

the only teacher in the CL process.

Ablation study results are detailed in Table IV and Table V. As we can see from the table, our method beats its ablations in Scenario 1/2/3/4 at both  $t = 2$ ,  $t = 3$ , and  $t = 4$ , which underscores that each component we propose is integral to the ultimate performance, hence proving themselves to be indispensable within our methodology.

### IV. WHY LLM WORKS: DISCUSSION AND CASE STUDY

A question one may ask is why using InstructBLIP as the additional teacher can significantly enhance the performance of the VQA task. Before answering the question, we want to point out that the multimodal LLM itself does not perform well when it tries to handle the surgical VQA task independently. In our experiments, we found that InstructBLIP tends to answer the task with “kidney”. This is understandable, as InstructBLIP is trained on general domain datasets, which means the model is more familiar with daily used words (e.g., kidney) than other surgical terms. However, we emphasize that *having poor performance when independently dealing with the surgical task does not mean few contributions under our multi-teacher CL framework*, as the information hidden in the LLM’s logits is also vital. The rest of this section illustrates how the LLM helps the CL training process with a case study.

At  $t = 2$ , experimental results show that the CL teacher model (trained at  $t = 1$  on EndoVis17) often confuses the “cutting” operation with the “idle” operation, leading to poor training outcomes when a conventional single-teacher framework is used. The “cutting” operation typically involves a surgical scissor. When the scissor is widely opened (Fig. 4a), the CL teacher correctly classifies the operation as “cutting”. However, when the scissor is not significantly opened (Fig. 4b), the CL teacher may misclassify the “cutting” operation as “idle”. This confusion is understandable, as a slightly opened scissor during “cutting” may resemble an “idle” one. However, a senior surgeon could clearly identify the operation as “cutting” based on the partially cut organ shown in Fig. 4b.

With our multi-teacher framework that uses LLM as a second teacher, the student model can effectively distinguish between “cutting” and “idle” operations. To understand how the LLM aids in the correct classification at  $t = 2$ , we



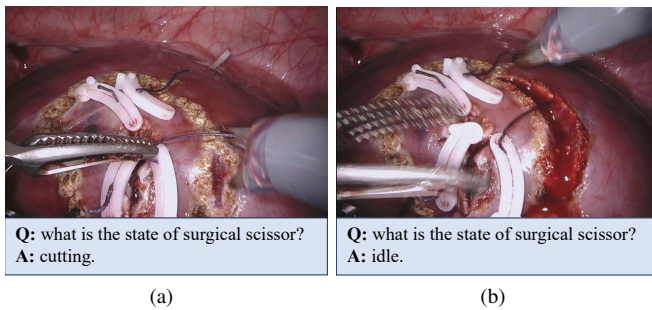


Figure 4: Two EndoVis18 images showing the cutting operation on a kidney. If the conventional signal-teacher CL approach were applied, the VQA model at  $t = 2$  would misclassify the second operation in (b) as “idle”.

examine the logits of both the conventional teacher and the LLM teacher during the learning process. Fig. 3a and Fig. 3b depict the logits of the conventional CL teacher and that of the LLM teacher for the studied “cutting” case. The old CL teacher assigns the highest logit value to “idle” and the second highest to “cutting”, indicating that the confusion between the two operations does exist. The LLM teacher attributes the highest logits to “kidney” and the second highest to “cutting”.

As we can see from the student’s logits presented in Fig. 3c, although neither the conventional CL model nor the LLM teacher can independently generate the correct answer, their combined decision, which is made by the weighted sum-up given in Eq. (2), can correctly identify the operation as “cutting”. This observation highlights the importance of our proposed multi-teacher CL framework with adaptive weights, which effectively utilizes the hidden information of the LLM’s logits to boost performance.

## V. CONCLUSION AND FUTURE WORK

This paper introduces a novel methodology to enhance the performance of surgical VQA tasks in surgical education under a CL setup. Through the proposed multi-teacher CL framework that utilizes a multimodal LLM to bridge the knowledge gap when facing domain shift and data imbalance, we effectively solve the catastrophic forgetting problem. Our innovative data processing scheme provides a method to extract logits from complex LLM embeddings, and our adaptive weight assignment approach ensures a balance between the domain-specific expertise of the old CL model and the strong generalization ability of the LLM. The application of these methods demonstrates compelling performance in tackling realistic surgical VQA tasks. Additionally, the new surgical domain VQA datasets that we have open-sourced offer a valuable resource for future research. Importantly, this paper puts forth a new research direction for leveraging LLMs in CL studies. The potential for improving continual learning VQA for clinical use remains significant. For future work, we plan to investigate how to decompose the representation into spatial space and temporal space, which has higher task-invariance, to further alleviate the model forgetting problem. Another potential direction is to integrate the multi-modal data, e.g.,

the kinematics data from the robot-assisted clinical systems, to advance the performance outcomes.

## REFERENCES

- [1] L. Seenivasan, M. Islam, A. K. Krishna, and H. Ren, “Surgical-VQA: Visual question answering in surgical scenes using transformer,” in *2022 MICCAI*. Springer, 2022, pp. 33–43.
- [2] L. Bai, M. Islam, and H. Ren, “Co-attention gated vision-language embedding for visual question localized-answering in robotic surgery,” *arXiv preprint arXiv:2307.05182*, 2023.
- [3] L. Seenivasan, M. Islam, G. Kannan, and H. Ren, “SurgicalGPT: End-to-end language-vision GPT for visual question answering in surgery,” *arXiv preprint arXiv:2304.09974*, 2023.
- [4] B. D. Nguyen, T.-T. Do, B. X. Nguyen, T. Do, E. Tjiputra, and Q. D. Tran, “Overcoming data limitation in medical visual question answering,” in *2019 MICCAI*. Springer, 2019, pp. 522–530.
- [5] Q. Wu, P. Wang, X. Wang, X. He, and W. Zhu, “Medical VQA,” in *Visual Question Answering: From Theory to Application*. Springer, 2022, pp. 165–176.
- [6] Y. Khare, V. Bagal, M. Mathew, A. Devi, U. D. Priyakumar, and C. Jawahar, “Mmbert: Multimodal Bert pretraining for improved medical vqa,” in *2021 ISBI*. IEEE, 2021, pp. 1033–1036.
- [7] H. Wang, Y. Jin, and L. Zhu, “Dynamic interactive relation capturing via scene graph learning for robotic surgical report generation,” in *2023 IEEE ICRA*, 2023, pp. 2702–2709.
- [8] Z. Zhao, Y. Jin, and P. Heng, “TraSeTR: Track-to-segment transformer with contrastive query for instance-level instrument segmentation in robotic surgery,” in *2022 IEEE ICRA*, 2022, pp. 11 186–11 193.
- [9] Z. Zhao, Y. Jin, B. Lu, C.-F. Ng, Q. Dou, Y.-H. Liu, and P.-A. Heng, “One to many: Adaptive instrument segmentation via meta learning and dynamic online adaptation in robotic surgical video,” in *2021 IEEE ICRA*, 2021, pp. 13 553–13 559.
- [10] Y. Jin, K. Cheng, Q. Dou, and P.-A. Heng, “Incorporating temporal prior from motion flow for instrument segmentation in minimally invasive surgery video,” in *Medical Image Computing and Computer Assisted Intervention (MICCAI) 2019*. Springer, 2019, pp. 440–448.
- [11] R. M. French, “Catastrophic forgetting in connectionist networks,” *Trends in cognitive sciences*, vol. 3, no. 4, pp. 128–135, 1999.
- [12] K. Shu, H. Li, J. Cheng, Q. Guo, L. Leng, J. Liao, Y. Hu, and J. Liu, “Replay-oriented gradient projection memory for continual learning in medical scenarios,” in *2022 IEEE BIBM*, 2022, pp. 1724–1729.
- [13] M. M. Derakhshani, I. Najdenkoska, T. van Sonsbeek, X. Zhen, D. Mahapatra, M. Worring, and C. G. Snoek, “Lifelong: A benchmark for continual disease classification,” in *2022 MICCAI*. Springer, 2022, pp. 314–324.
- [14] M. Lenga, H. Schulz, and A. Saalbach, “Continual learning for domain adaptation in chest x-ray classification,” in *Medical Imaging with Deep Learning*. PMLR, 2020, pp. 413–423.
- [15] Z. Li and D. Hoiem, “Learning without forgetting,” *IEEE Trans. Pattern Anal. Mach. Intell.*, vol. 40, no. 12, pp. 2935–2947, 2017.
- [16] J. Kirkpatrick, R. Pascanu, N. Rabinowitz, J. Veness, G. Desjardins, A. A. Rusu, K. Milan, J. Quan, T. Ramalho, A. Grabska-Barwinska et al., “Overcoming catastrophic forgetting in neural networks,” *Proc. Nat. Acad. Sci.*, vol. 114, no. 13, pp. 3521–3526, 2017.
- [17] L. Bai, M. Islam, and H. Ren, “Revisiting distillation for continual learning on visual question localized-answering in robotic surgery,” *arXiv preprint arXiv:2307.12045*, 2023.
- [18] M. Phuong and C. Lampert, “Towards understanding knowledge distillation,” in *2019 ICML*. PMLR, 2019, pp. 5142–5151.
- [19] C. Simon, M. Faraki, Y.-H. Tsai, X. Yu, S. Schultze, Y. Suh, M. Harandi, and M. Chandraker, “On generalizing beyond domains in cross-domain continual learning,” in *2022 CVPR*, 2022, pp. 9265–9274.
- [20] T. Diethe, T. Borchert, E. Thereska, B. Balle, and N. Lawrence, “Continual learning in practice,” *arXiv preprint arXiv:1903.05202*, 2019.
- [21] C. D. Kim, J. Jeong, and G. Kim, “Imbalanced continual learning with partitioning reservoir sampling,” in *2020 ECCV*. Springer, 2020, pp. 411–428.
- [22] A. Chrysakakis and M.-F. Moens, “Online continual learning from imbalanced data,” in *2020 ICML*. PMLR, 2020, pp. 1952–1961.
- [23] A. Belyaeva, J. Cosentino, F. Hormozdiari, C. Y. McLean, and N. A. Furlotte, “Multimodal LLMs for health grounded in individual-specific data,” *arXiv preprint arXiv:2307.09018*, 2023.
- [24] Y. Du, S. C. Liew, K. Chen, and Y. Shao, “The power of large language models for wireless communication system development: A case study on FPGA platforms,” *arXiv preprint arXiv:2307.07319*, 2023.

- [25] Z. Guo, R. Zhang, X. Zhu, Y. Tang, X. Ma, J. Han, K. Chen, P. Gao, X. Li, H. Li *et al.*, “Point-bind & point-LLM: Aligning point cloud with multi-modality for 3D understanding, generation, and instruction following,” *arXiv preprint arXiv:2309.00615*, 2023.
- [26] H. Cui, Y. Du, Q. Yang, Y. Shao, and S. C. Liew, “LLMind: Orchestrating AI and IoT with LLMs for complex task execution,” *arXiv preprint arXiv:2312.09007*, 2023.
- [27] A. J. Thirunavukarasu, D. S. J. Ting, K. Elangovan, L. Gutierrez, T. F. Tan, and D. S. W. Ting, “Large language models in medicine,” *Nature medicine*, pp. 1–11, 2023.
- [28] H. Nori, N. King, S. M. McKinney, D. Carignan, and E. Horvitz, “Capabilities of GPT-4 on medical challenge problems,” *arXiv preprint arXiv:2303.13375*, 2023.
- [29] S. Min, X. Lyu, A. Holtzman, M. Artetxe, M. Lewis, H. Hajishirzi, and L. Zettlemoyer, “Rethinking the role of demonstrations: What makes in-context learning work?” *arXiv preprint arXiv:2202.12837*, 2022.
- [30] S. Min, M. Lewis, L. Zettlemoyer, and H. Hajishirzi, “Metaicl: Learning to learn in context,” *arXiv preprint arXiv:2110.15943*, 2021.
- [31] K. Chen, J. Li, K. Wang, Y. Du, J. Yu, J. Lu, G. Chen, L. Li, J. Qiu, Q. Fang *et al.*, “Towards an automatic ai agent for reaction condition recommendation in chemical synthesis,” *arXiv preprint arXiv:2311.10776*, 2023.
- [32] K. Chen, H. Cao, J. Li, Y. Du, M. Guo, X. Zeng, L. Li, J. Qiu, P. A. Heng, and G. Chen, “An autonomous large language model agent for chemical literature data mining,” *arXiv preprint arXiv:2402.12993*, 2024.
- [33] O. Rubin, J. Herzig, and J. Berant, “Learning to retrieve prompts for in-context learning,” *arXiv preprint arXiv:2112.08633*, 2021.
- [34] J. Gou, B. Yu, S. J. Maybank, and D. Tao, “Knowledge distillation: A survey,” *International Journal of Computer Vision*, vol. 129, pp. 1789–1819, 2021.
- [35] X. Dai, Z. Jiang, Z. Wu, Y. Bao, Z. Wang, S. Liu, and E. Zhou, “General instance distillation for object detection,” in *2021 CVPR*, 2021, pp. 7842–7851.
- [36] D. Wenliang, L. Junnan, L. Dongxu, T. Anthony Meng Huat, Z. Junqi, W. Weisheng, L. Boyang, F. Pascale, and H. Steven, “InstructBLIP: Towards general-purpose vision-language models with instruction tuning,” *arXiv preprint arXiv:2305.06500*, 2023.
- [37] H. W. Chung, L. Hou, S. Longpre, B. Zoph, Y. Tay, W. Fedus, E. Li, X. Wang, M. Dehghani, S. Brahma *et al.*, “Scaling instruction-finetuned language models,” *arXiv preprint arXiv:2210.11416*, 2022.
- [38] F. Thabtah, S. Hammoud, F. Kamalov, and A. Gonsalves, “Data imbalance in classification: Experimental evaluation,” *Information Sciences*, vol. 513, pp. 429–441, 2020.
- [39] L. Maier-Hein, M. Eisenmann, D. Sarikaya, K. März, T. Collins, A. Malpani, J. Fallert, H. Feussner, S. Giannarou, P. Mascagni *et al.*, “Surgical data science—from concepts toward clinical translation,” *Medical image analysis*, vol. 76, p. 102306, 2022.
- [40] Z.-L. Ni, G.-B. Bian, Z.-G. Hou, X.-H. Zhou, X.-L. Xie, and Z. Li, “Attention-guided lightweight network for real-time segmentation of robotic surgical instruments,” in *2020 ICRA*. IEEE, 2020, pp. 9939–9945.
- [41] J. Liu, X. Guo, and Y. Yuan, “Graph-based surgical instrument adaptive segmentation via domain-common knowledge,” *IEEE Trans. Med. Imaging*, vol. 41, no. 3, pp. 715–726, 2021.
- [42] L. Bai, M. Islam, L. Seenivasan, and H. Ren, “Surgical-VQLA: Transformer with gated vision-language embedding for visual question localized-answering in robotic surgery,” *arXiv preprint arXiv:2305.11692*, 2023.
- [43] E. Rojas-Muñoz, K. Couperus, and J. Wachs, “Daisi: database for AI surgical instruction,” *arXiv preprint arXiv:2004.02809*, 2020.
- [44] D. R. Yates, C. Vaessen, and M. Roupert, “From Leonardo to Da Vinci: the history of robot-assisted surgery in urology,” *BJU international*, vol. 108, no. 11, pp. 1708–1713, 2011.
- [45] J. C.-Y. Ngu, C. B.-S. Tsang, and D. C.-S. Koh, “The Da Vinci Xi: a review of its capabilities, versatility, and potential role in robotic colorectal surgery,” *Robotic Surgery: Research and Reviews*, pp. 77–85, 2017.
- [46] K.-Y. Lei, W.-J. Xie, S.-Q. Fu, M. Ma, and T. Sun, “A comparison of the Da Vinci Xi vs. Da Vinci Si surgical systems for radical prostatectomy,” *BMC surgery*, vol. 21, pp. 1–6, 2021.
- [47] R. Liu, Q. Liu, G. Zhao, Z. Zhao, M. Li, and Y. Gao, “Single-port robotic pancreatic surgery using the Da Vinci SP system: A retrospective study on prospectively collected data in a consecutive patient cohort,” *International Journal of Surgery*, vol. 104, p. 106782, 2022.
- [48] N. Ragavan, S. Bharathkumar, P. Chirravur, S. Sankaran, and A. Mottrie, “Evaluation of Hugo RAS system in major urologic surgery: our initial experience,” *Journal of Endourology*, vol. 36, no. 8, pp. 1029–1035, 2022.
- [49] S. W. Lei, D. Gao, J. Z. Wu, Y. Wang, W. Liu, M. Zhang, and M. Z. Shou, “Symbolic replay: Scene graph as prompt for continual learning on vqa task,” in *2023 AAAI*, vol. 37, no. 1, 2023, pp. 1250–1259.
- [50] S. Zhang and R. S. Sutton, “A deeper look at experience replay,” *arXiv preprint arXiv:1712.01275*, 2017.
- [51] A. Chaudhry, P. K. Dokania, T. Ajanthan, and P. H. Torr, “Riemannian walk for incremental learning: Understanding forgetting and intransigence,” in *2018 ECCV*, 2018, pp. 532–547.
- [52] F. Huszár, “Note on the quadratic penalties in elastic weight consolidation,” *Proc. Nat. Acad. Sci.*, vol. 115, no. 11, pp. E2496–E2497, 2018.